Supporting Information:
Stress-Induced Martensitic Transformation in Na_3YCl_6

Akira Miura[a+*], Koki Muraoka[b+*], Kotaro Maki[c], Saori Kawaguchi[d], Kazuhiro Hikima[e], Hiroyuki Muto[e,f], Atsunori Matsuda[e], Ichiro Yamane[c], Toshihiro Shimada[a], Hiroaki Ito[c], Yoshikazu Mizuguchi[g], Chikako Moriyoshi,[h] Hiroshi Nakajima,[i] Shigeo Mori,[i] Hiroshi Oike,[j] Akira Nakayama,[b] Wenhao Sun,[k] Nataly Carolina Rosero-Navarro,[a,l], Kiyoharu Tadanaga[a]

[+]contributed equally

[a] Faculty of Engineering, Hokkaido University, Kita 13, Nishi 8, Sapporo 060-8628, Japan

[b] Department of Chemical System Engineering, The University of Tokyo, 7-3-1 Hongo, Bunkyo-ku, Tokyo 113-8656, Japan

[c] Graduate School of Chemical Science and Engineering, Hokkaido University, Kita 13, Nishi 8, Sapporo 060-8628, Japan

[d] Japan Synchrotron Radiation Research Institute, Sayo, Hyogo 679-5198, Japan

[e] Department of Electrical and Electronic Information Engineering, Toyohashi University of Technology, 1-1 Hibarigaoka, Tempaku, Toyohashi, Aichi 441-8580, Japan

[f] Institute of Liberal Arts and Sciences, Toyohashi University of Technology, 1-1 Hibarigaoka, Tempaku, Toyohashi, Aichi 441-8580, Japan

[g] Department of Physics, Tokyo Metropolitan University, Hachioji 192-0397, Japan

[h] Graduate School of Advanced Science and Engineering, Hiroshima University, 1-3-1 Kagamiyama, Higashihiroshima, 739-8526, Japan

[i] Department of Materials Science, Graduate School of Engineering, Osaka Metropolitan University, 1-1 Gakuen-cho, Naka-ku, Sakai, Osaka 599-8531, Japan

[j] PRESTO, Japan Science and Technology Agency, 4-1-8 Honcho, Kawaguchi 332-0012, Japan

[k] Department of Materials Science, University of Michigan, Ann Arbor, Michigan 48109, United States

[l] Instituto de Cerámica y Vidrio (CSIC), Campus de Cantoblanco, 28049, Madrid, Spain

mail: amirua@eng.hokudai.ac.jp(AMiura) , muraok_k@chemsys.t.u-tokyo.ac.jp(KMuraoka)

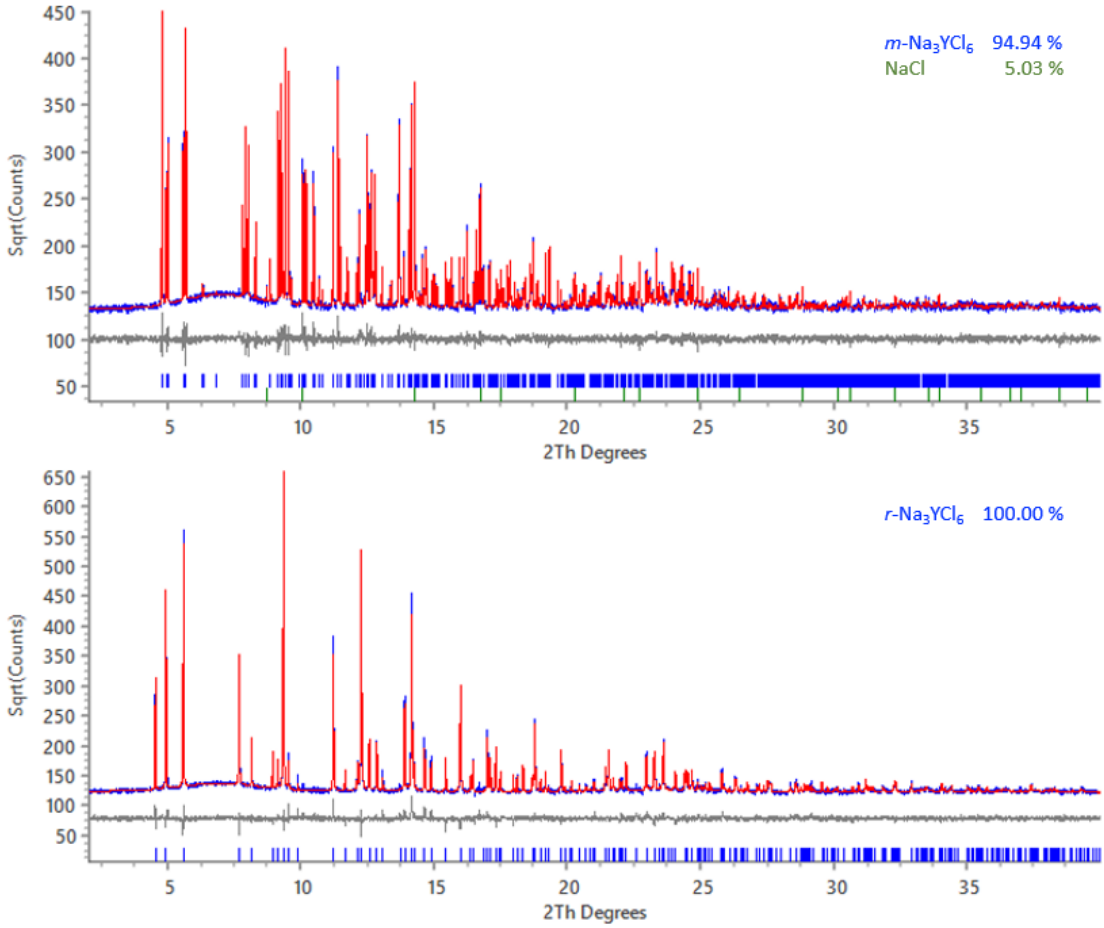

Figure S1 Rietveld refinement profiles of *m*- and *r*-Na_3YCl_6 acquired by synchrotron XRD with the wavelength of 0.496480 Å.

Table S1 Crystallographic data of Na_3YCl_6 determined by SXRD.

	m-Na_3YCl_6 (exp)	*r*-Na_3YCl_6 (exp)	*m*-Na_3YCl_6 ICSD#59886	*r*-Na_3YCl_6 ICSD#300258
a (Å)	6.86436(5)	6.96849(5)	6.8558(9)	6.973(1)
b (Å)	7.26180(5)	= *a*	7.2550(10)	= *a*
c (Å)	10.15659 (10)	18.67687(18)	10.1444(13)	18.684(4)
α (°)	90	90	90	90
β (°)	90.8249 (5)	90	90.869(3)	90
γ (°)	90	120	90	120
Lattice volume / Na_3YCl_6 unit (Å^3)	253.12	261.81	252.26	262.25

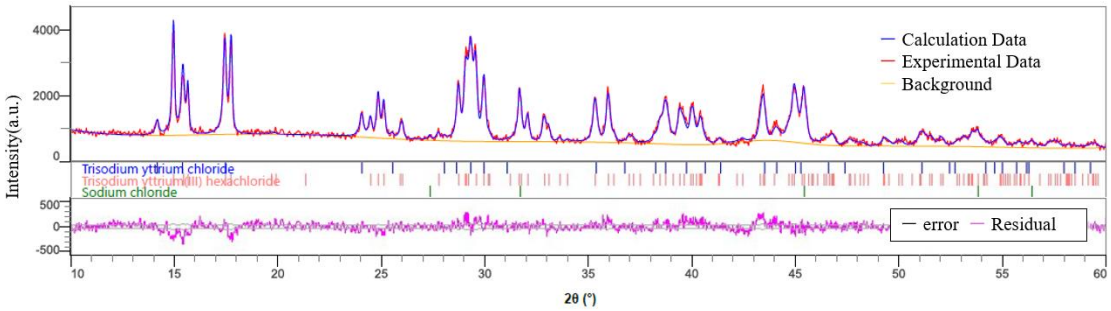

Figure S2 Rietveld profile of *m*-Na_3YCl_6 pellet after applying the anisotropic pressure of 0.3 GPa: R_{wp}=7.57 %, R_p=6.00 %.

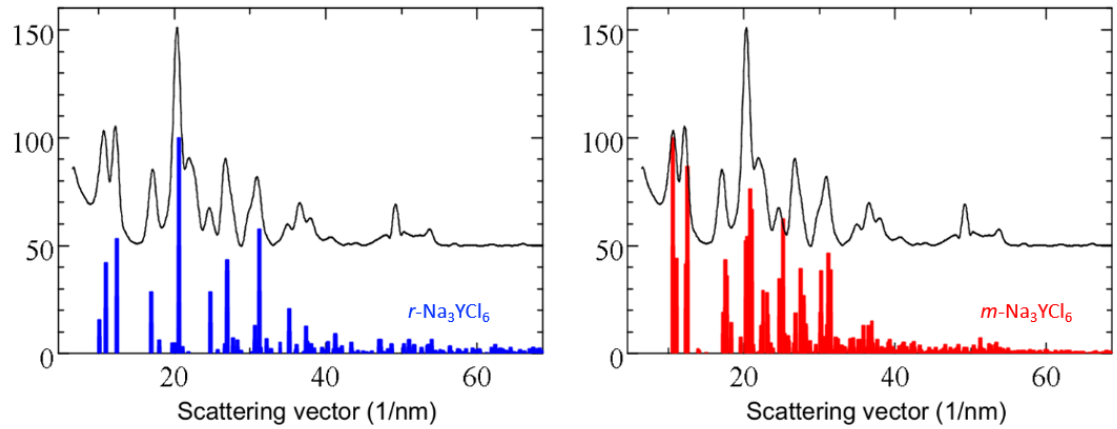

Figure S3: Integrated electron diffraction of mechanically stimulated Na_3YCl_6.

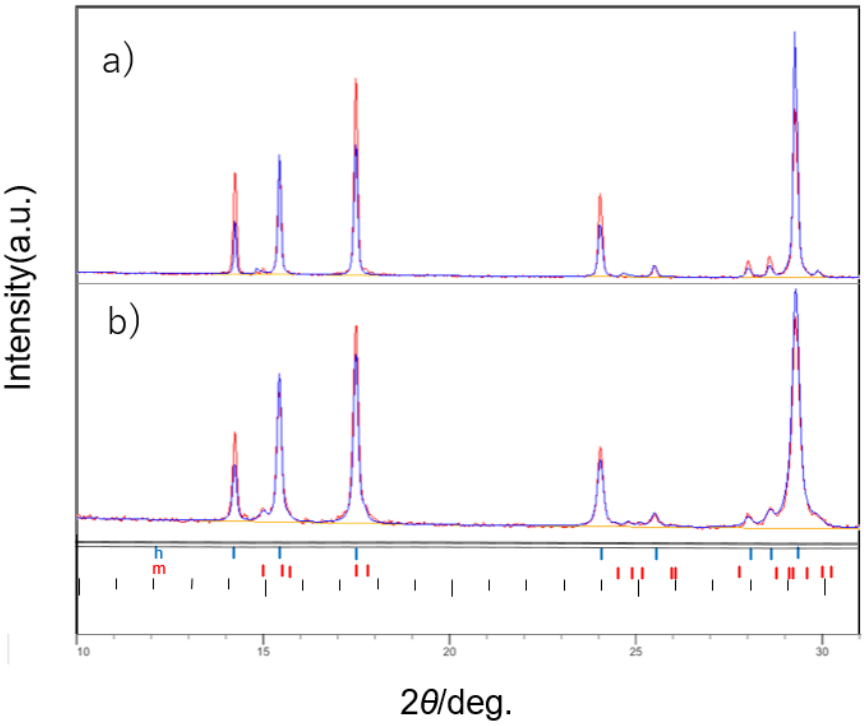

Figure S4 Phase transformation of *r*-Na_3YCl_6 triggered by mechanical stimulation. XRD patterns of ***r***-Na_3YCl_6 (a) before mechanical stimulation, (b) after applying anisotropic pressure of 0.3 GPa.

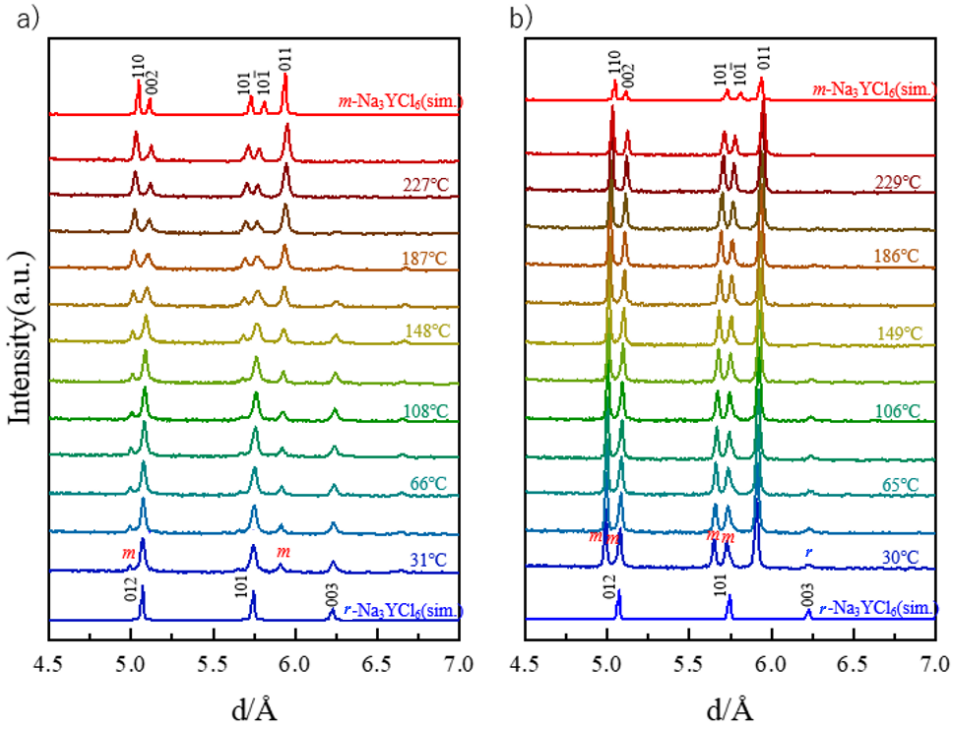

Figure S5 In-situ XRD patterns of *r*-Na_3YCl_6 at various temperatures upon heating.
a) as-synthesized *r*-Na_3YCl_6. b) *r*-Na_3YCl_6 formed by uniaxial pressurization.

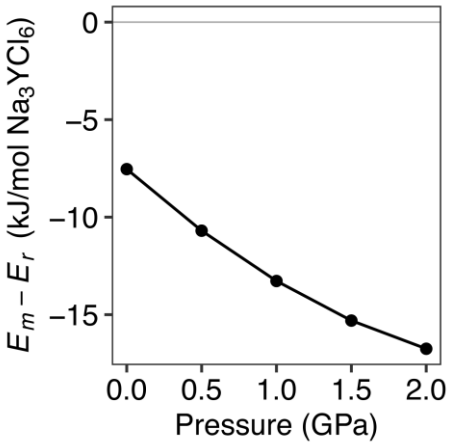

Figure S6 Variation of the energy difference ($E_m - E_r$) between *m*-phase and *r*-phase as a function of pressure. Pressures were applied under isotropic conditions.

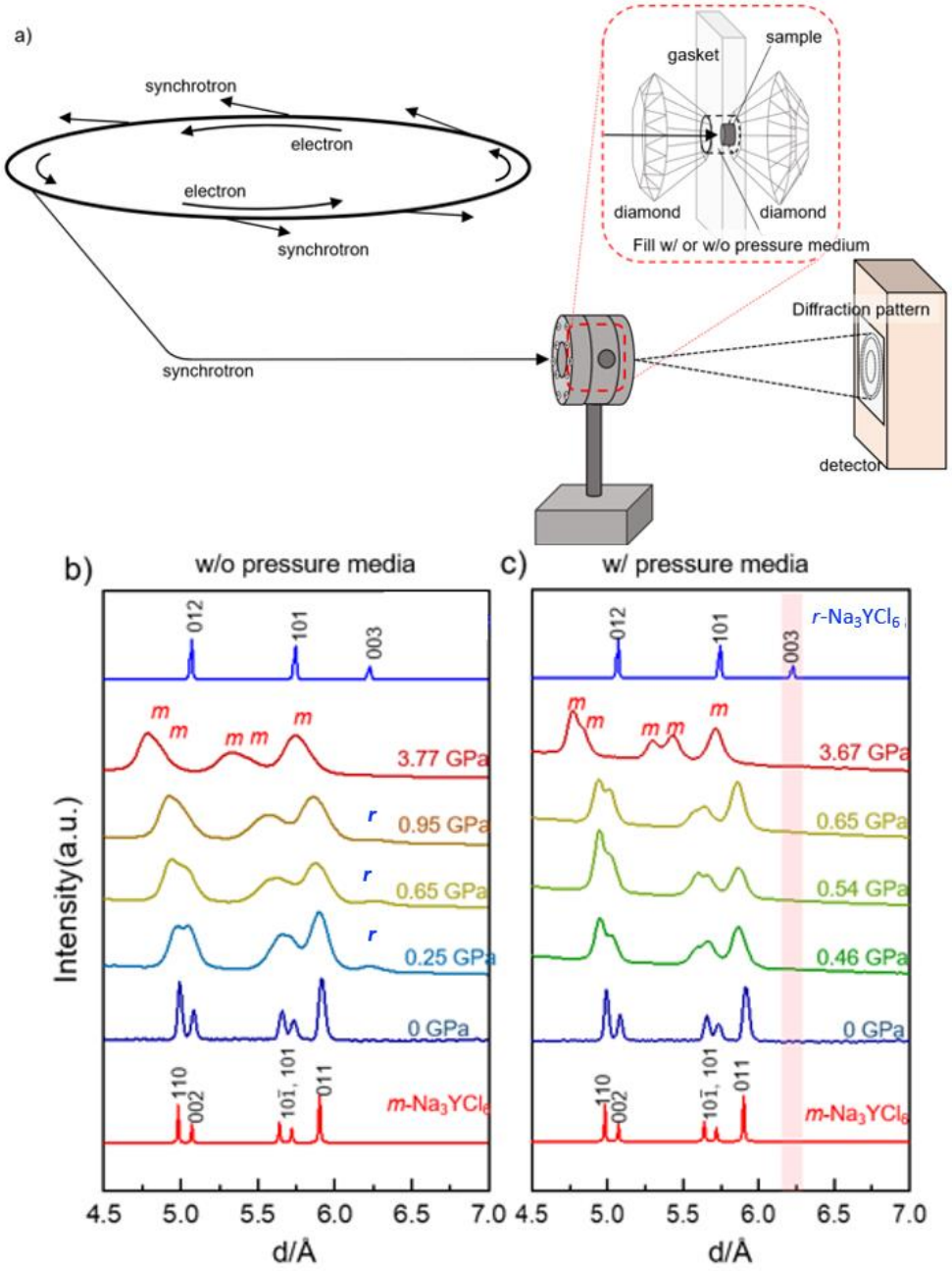

Figure S7 Pressure-dependent phase transformation of *m*-Na_3YCl_6. a) Schematic of the setting of in-situ XRD measurement. b) In-situ XRD pattern during anisotropic pressurization. (w/o pressure medium.) c) In-situ XRD pattern during isostatic pressurization. (w/ pressure medium.)

Table S2: Crystallographic data of Na_3YCl_6 structures optimized by PFP.

	m-Na_3YCl_6	*r*-1-Na_3YCl_6	*r*-2-Na_3YCl_6
a (Å)	6.934	7.114	7.029
b (Å)	7.332	7.114	7.029
c (Å)	10.352	18.94	19.701
α (°)	90.00	90.00	90.00
β (°)	90.69	90.00	90.00
γ (°)	90.00	120.00	120.00
Lattice volume / Na_3YCl_6 unit (Å^3)	263.1	276.7	281.0

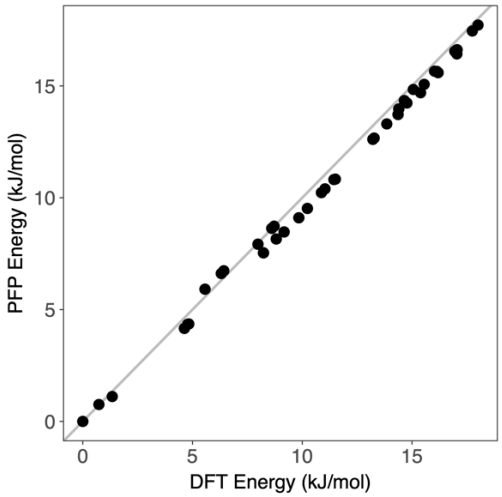

Figure S8 The correlation between the relative energy computed by PFP and the relative energy computed by DFT for images that were observed in G-SSNEB without any pressure, as well as under isotropic and anisotropic pressures of 0.5 GPa. The root mean squared error was 0.52 kJ/mol (Na_3YCl_6), the mean absolute error was 0.47 kJ/mol (Na_3YCl_6), and the R^2 value was 0.996.

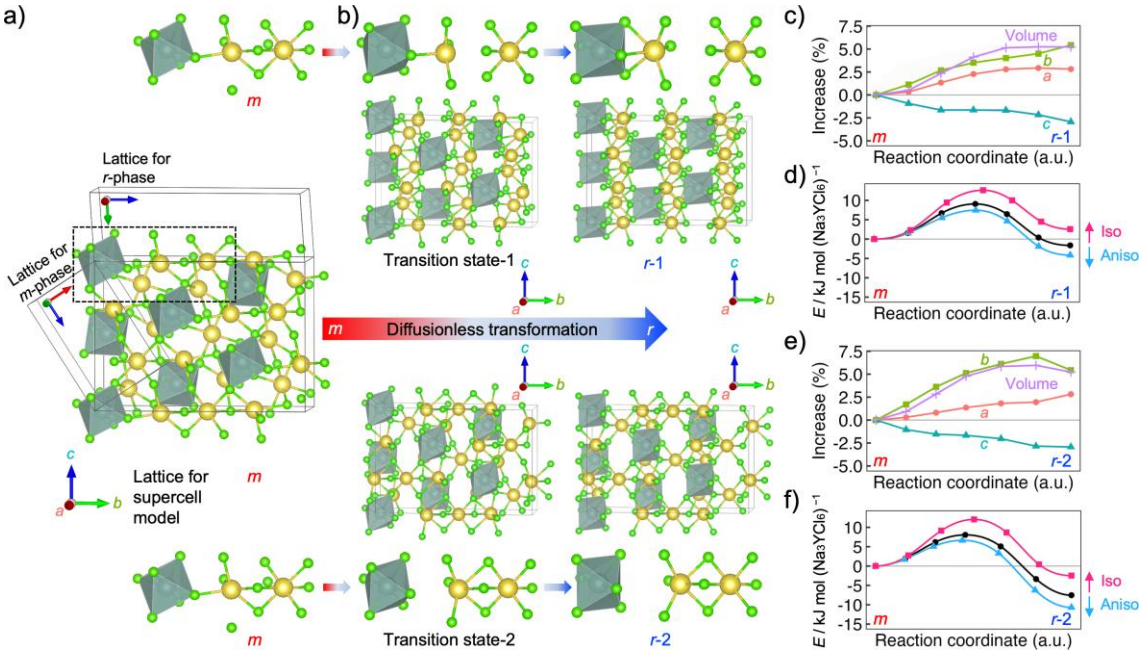

Figure S9 Calculated Martensitic transformation pathways under no pressure, isotropic pressure (0.5 GPa), and anisotropic pressure along the *c*-axis (0.5 GPa). a) The relationships between the *m*-phase, the *r*-phase and the supercell model used for the calculations. Na atoms undergo the *m*-to-*r*-1 transformation by moving along the grey arrows, while they follow the yellow arrows during the *m*-to-*r*-2 transformation. a, b) Diffusionless transformation pathways from the *m*-phase to the *r*-1 phase (top) and from the *m*-phase to the *r*-2 phase (bottom) under no pressure. c, e) The lattice constants and volumes undergo a change during the phase transformation from *m* to *r*-1 (c) and *m* to *r*-2 (e) at zero pressure. As the phase transformation proceeds, the volume and the lattice constants of *a* and *b* increase, while the lattice constant of *c* decreases. d, f) Energy profiles of the phase transformation from the *m*-phase to the *r*-1 phase (d) and from the *m*-phase to the *r*-2 phase (f). Black circles represent the transformation without pressure, while blue triangles and red squares represent the transformation under anisotropic and isotropic pressure, respectively.

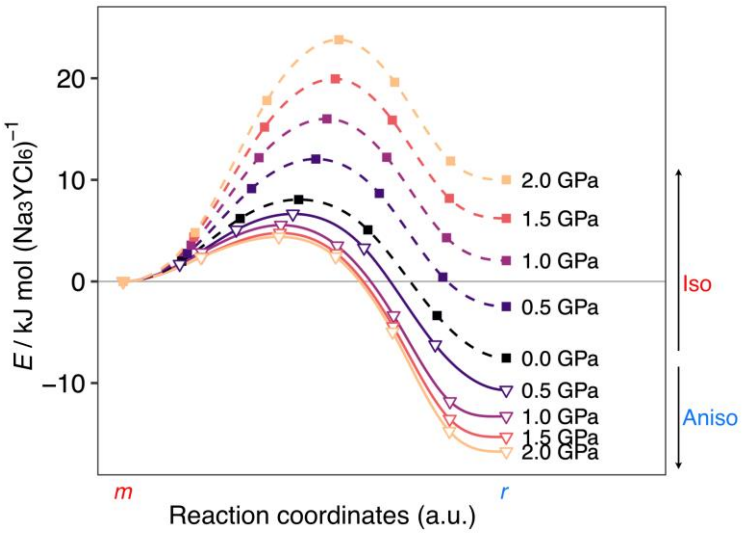

Figure S10 Energy profiles of the phase transformation from the *m*-phase to the *r*-phase under different pressure conditions. Filled squares represent the transformation under isotropic pressure, while blank triangles represent the transformation under anisotropic pressurization. Anisotropic pressurization consistently reduced the activation energy, further stabilizing the *r*-phase, which suggests its effectiveness in promoting the *m*-to-*h* transformation. Conversely, isotropic pressurization appears to inhibit this transformation by increasing the activation energy. Additionally, applying isotropic pressurization alters the phase stability: the *r*-phase becomes more stable under conditions of high isotropic pressurization.